



ELSEVIER

Surface Science 314 (1994) 353–364

surface science

## HV-TEM in-situ investigations of the tip shape of indium liquid metal ion emitter

B. Praprotnik<sup>a</sup>, W. Driesel<sup>b</sup>, Ch. Dietzsch<sup>b</sup>, H. Niedrig<sup>\*,a</sup>

<sup>a</sup> Technische Universität Berlin, Optisches Institut, Strasse des 17. Juni 135, 10623 Berlin, Germany

<sup>b</sup> Max-Planck-Institut für Mikrostrukturphysik Halle, Weinberg 2, 06120 Halle, Germany

(Received 21 February 1994; accepted for publication 5 April 1994)

### Abstract

An indium liquid metal ion emitter has been observed in-situ in the Halle 1 MeV electron transmission microscope. The investigations have shown deviations from the theoretical shape of the Taylor cone. A linear dependence of the opening angle and the extension of the apex from the emission current was stated.

With emission currents greater than 10  $\mu\text{A}$  an extension of the cone's apex had been observed. For the first time the dynamical behaviour of a liquid metal ion emitter had been investigated. Microdroplet emission had been observed in the cone's surrounding. The radii of microdroplets show a dependence from the field strength and vary between 0.04 and 1.4  $\mu\text{m}$ . Some spatial instabilities of the Taylor cone had been noticed.

### 1. Introduction

Liquid metal ion sources are known as ion emitters of small size with high source brightness. They are frequently used as ion probes for material preparation, in micro-mechanics or for maskless implantation [1,2]. The high field strength demanded for ion emission is achieved by the formation of a liquid metal cone due to electrostatic forces.

The electrohydrodynamic processes which occur at the liquid metal tip were described by Rayleigh [3], Zeleny [4] and Taylor [5]. Based on the results according to Taylor's theory, in which a material independent, unchangeable cone forms at the tip after exceeding a critical voltage  $U_T$ ,

Gomer [6] developed the first theory of liquid metal ion sources. Later Kingham and Swanson [7] developed a dynamic theory which also considers liquid flow and space charge effects. This theory was recently improved by other authors [8].

The greatest problem in testing and developing liquid metal ion emitter (LMIE) theories is the lack of experimental data which describe the shape of the LMIE in dependence from working parameters. The first images of the liquid metal cone were made by Benassayag, Sudraud and Jouffrey [9]. They have investigated a gallium-LMIE in a 3 MeV transmission electron microscope (TEM).

The purpose of this paper is to present in-situ images of the surface shape of an indium-LMIE obtained with the 1 MeV TEM (JEOL JEM HV) of the Max-Planck-Institut für Mikrostrukturphysik Halle.

\* Corresponding author. Fax: +30 31 426 888.

## 2. Experimental aspects

There are two possibilities for observing the shape of a liquid metal cone:

- The emitter is being cooled below the solidification temperature during emission. If the cooling proceeds quickly enough the shape of the liquid metal cone can be frozen and represented in the transmission microscope. The disadvantage of this method is that the smallest structures

round off. This rounding off is caused by the high electrical field needed for the emission [8].

- The LMIE is being observed in a high-voltage electron microscope (HV-TEM) during emission. This method makes more precise statements on the surface shape and on the dynamics of the emission process possible.

All major parts of the LMIE including the extraction electrode can easily be fitted into the object chamber of the HV-TEM. For the experi-

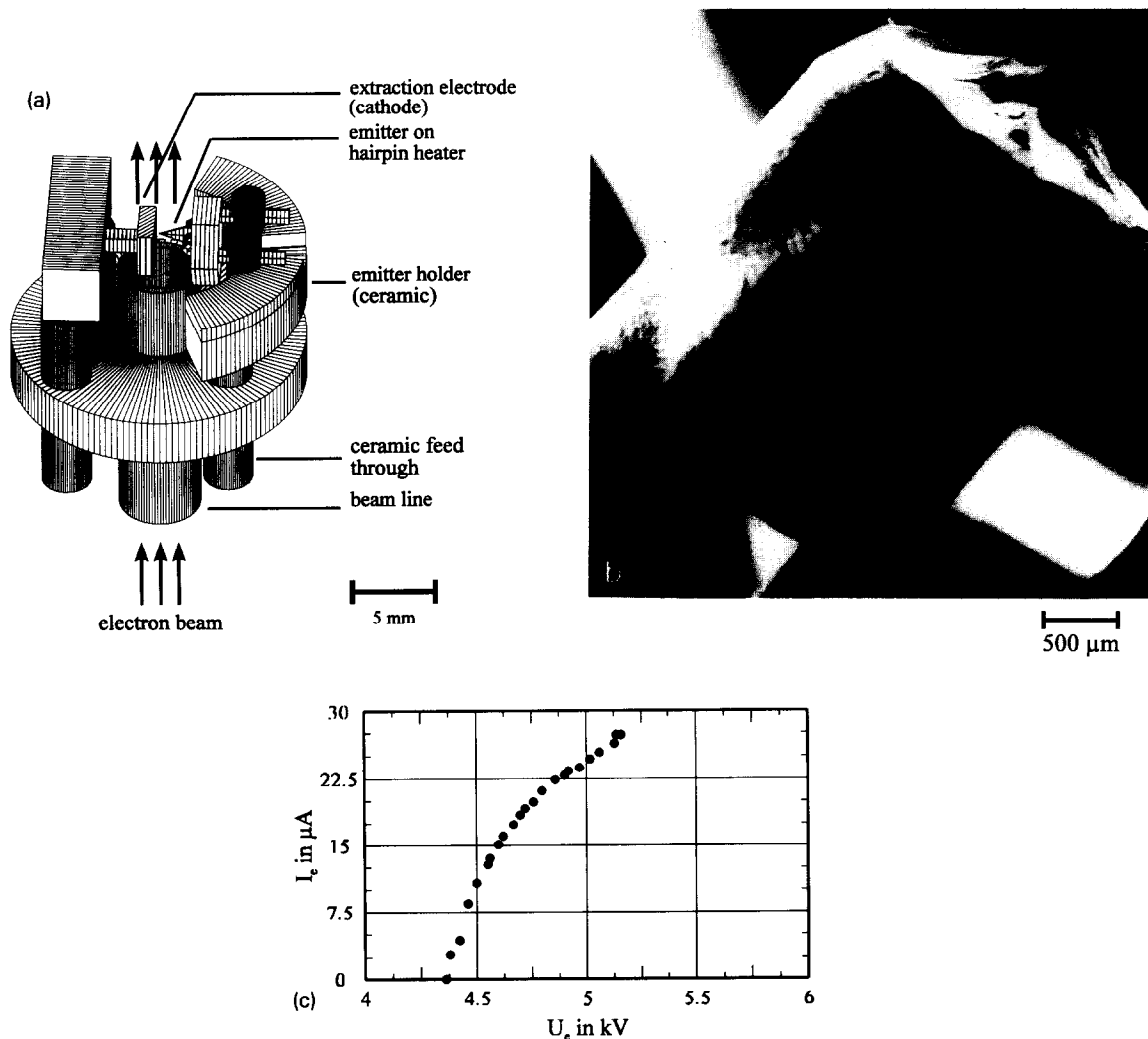


Fig. 1. (a) Specimen holder used for in-situ observations of indium-LMIS; (b) An indium liquid metal ion emitter used for in-situ investigations; (c) Emission current extraction voltage characteristics.

ments a special specimen holder, which enabled the installation of the emitter with electrical connections into the object level of the HV-TEM, had been built (Fig. 1a). The images of the LMIE-surface shape were taken with an acceleration voltage  $U_b$  of 1 MV. The shadow projection could be taken by a photo or video camera.

The most important part of the emitter (Fig. 1b) is the tungsten tip. The tip was electrolytically etched in KOH. The desired tip radius can be achieved by variation of the immersion depth and of the etching current [10]. Tips with radii between 0.5 and 1  $\mu\text{m}$  were used, the surface of the etched tip is roughened by short etching with AC voltage and is bonded to a 0.2 mm tungsten hairpin heater. A steel capsule is pushed over and fitted to the tungsten hairpin heater, the capsule serves as the reservoir for the liquid metal. A plane extraction electrode is situated opposite the emitter, the distance between these two elements is adjustable within 0 to 1 mm.

The emitter is electrolytically coated with indium. Then, small pieces of indium are put into the reservoir and melted in the high vacuum until the whole tip is coated. Finally, the emitter is tested for emission capability. The necessary temperature is adjusted for each tip by varying the current through the tungsten hairpin heater. The exact temperature has not been measured. When the desired temperature is reached, the voltage on the emitter  $U_e$  is raised (max. 7 kV) until the emission starts. The emission current is measured in the collector circuit (at the extraction electrode). The correction of the emission current  $I_e$  due to incoming electron current is not done. The contribution of the incoming electron current ( $< 0.2 \mu\text{A}$ ) is smaller than the measuring error

( $\Delta I_e = \pm 0.3 \mu\text{A}$ ). The voltage  $U_e$  also serves for adjusting the emission current.

For the measurements represented in this paper, a tip with the radius  $r = 1.0 \mu\text{m}$  and a distance to the extraction electrode of 0.42 mm was used. To characterize the liquid metal flow along the tungsten tip [24], the current voltage curve is measured for the emitter used in the in-situ experiments (Fig. 1c).

The high electrical field near the emission tip leads to a deviation of the imaging electron-trajectories in the HV-TEM. In order to estimate this error approximately, Benassayag et al. [9] suggested to consider this system as a thin wire of radius  $r$  centred between two grounded capacitor plates (electron optical biprism). The wire carries the voltage  $U_e$ . An electron with the mass  $m$  moving with the kinetic energy  $U_b e$  in little distance to the wire, is deflected by the angle  $\gamma$ . According to Möllenstedt [11] the deflection angle can be expressed as:

$$\gamma = \frac{U_e}{2U_b \ln(R/r)}, \quad (1)$$

where  $R$  is the distance between the capacitor plates. The electron velocity is so high that a relativistic correction is needed. This correction was calculated according to the approach of Landau et al. [12]. With this correction the deflection angle is defined as:

$$\gamma = \frac{U_e}{2U_b \ln(R/r)} \times \frac{1 + (2U_b e/mc^2) + (U_b^2 e^2/m^2 c^4)}{1 + (U_b e/2mc^2)}. \quad (2)$$

Table 1 lists the deflection angles  $\gamma$  for different

Table 1

The deflection angles  $\gamma$  for different tip radii  $r$  and the acceleration voltages of electrons  $U_b$  calculated with formula (2); for the wire voltage at the emitter tip  $U_e = 5 \text{ kV}$  was exemplarily chosen

$\gamma$ (rad)	$r$ ( $\mu\text{m}$ )					
$U_b$ (MV)	10	5	1	0.5	0.1	0.05
0.1	$4.17 \times 10^{-3}$	$3.82 \times 10^{-3}$	$3.20 \times 10^{-3}$	$2.99 \times 10^{-3}$	$2.59 \times 10^{-3}$	$2.45 \times 10^{-3}$
1	$8.17 \times 10^{-4}$	$7.48 \times 10^{-4}$	$6.27 \times 10^{-4}$	$5.86 \times 10^{-4}$	$5.08 \times 10^{-4}$	$4.81 \times 10^{-4}$
3	$6.73 \times 10^{-5}$	$6.17 \times 10^{-5}$	$5.17 \times 10^{-5}$	$4.83 \times 10^{-5}$	$4.19 \times 10^{-5}$	$3.96 \times 10^{-5}$

tip radii  $r$  and electron acceleration voltages  $U_b$  calculated with formula (2). A voltage of  $U_e = 5$  kV at the emitter tip was exemplarily chosen.

Table 1 makes evident that with increasing acceleration voltage  $U_b$ , a considerable decrease of the electron deflection is possible. Thus, the use of 1

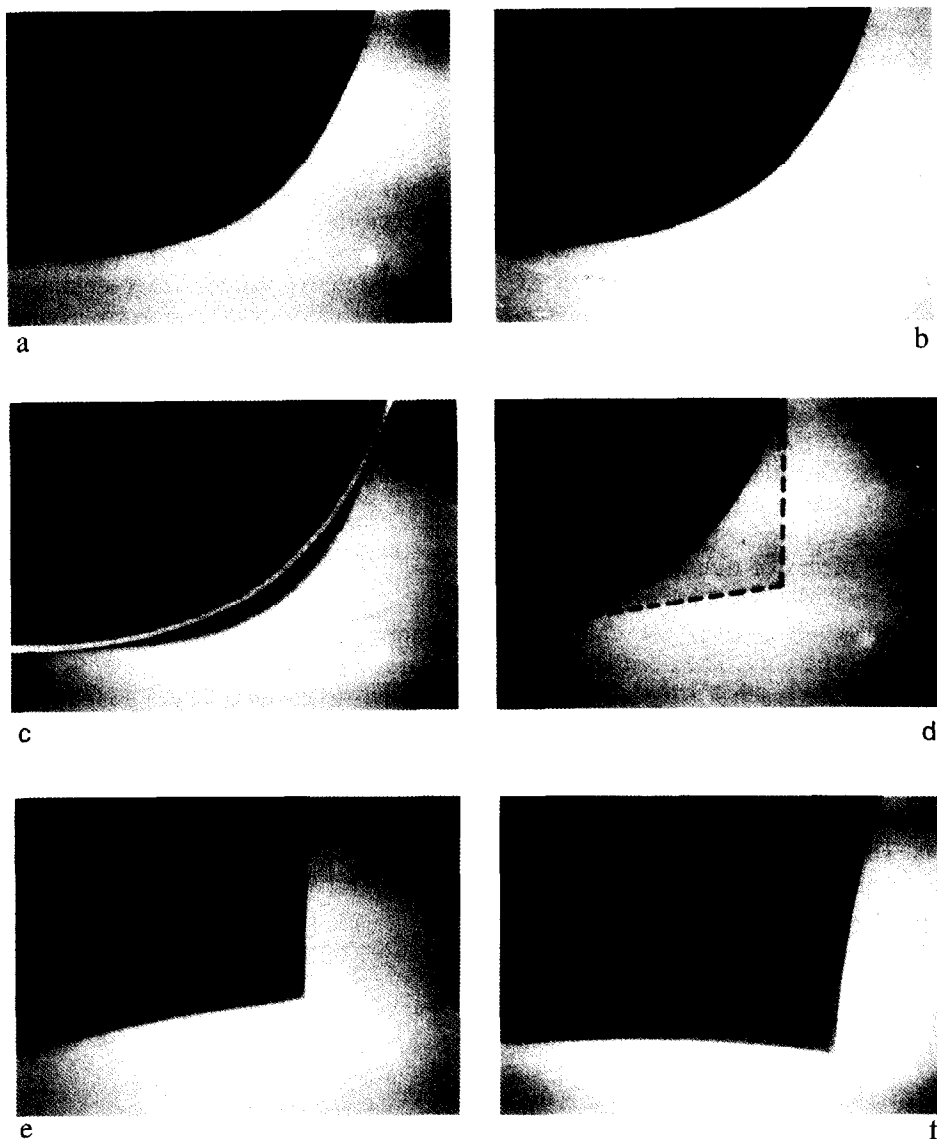


Fig. 2. Formation of the Taylor cone. The images are taken from the videofilm and temporally ordered: (a) starting image; (b) surface shape after 10.5 s (no shape changes); (c) surface shape after 10.86 s (the surface formed a bump – the initial shape is superimposed as a white line); (d) surface shape after 10.88 s (Taylor cone already formed – marked with dashed line); (e) surface shape after 10.94 s, (f) surface shape at stable emission (after 11 s).

MV acceleration voltage results in an improvement of about 5 in comparison with 100 kV acceleration voltage.

Comparing the images of a tip with a voltage of  $U_e = 5$  kV and without voltage ( $U_e = 0$  kV) one could estimate the imaging error of approximately 20 nm. This roughly corresponds with the

value given by Benassayag et al. [9] for their apparatus.

### 3. Formation and shape of the Taylor cone

Before forming a Taylor cone, the coated tip shows a spherical surface which does not change

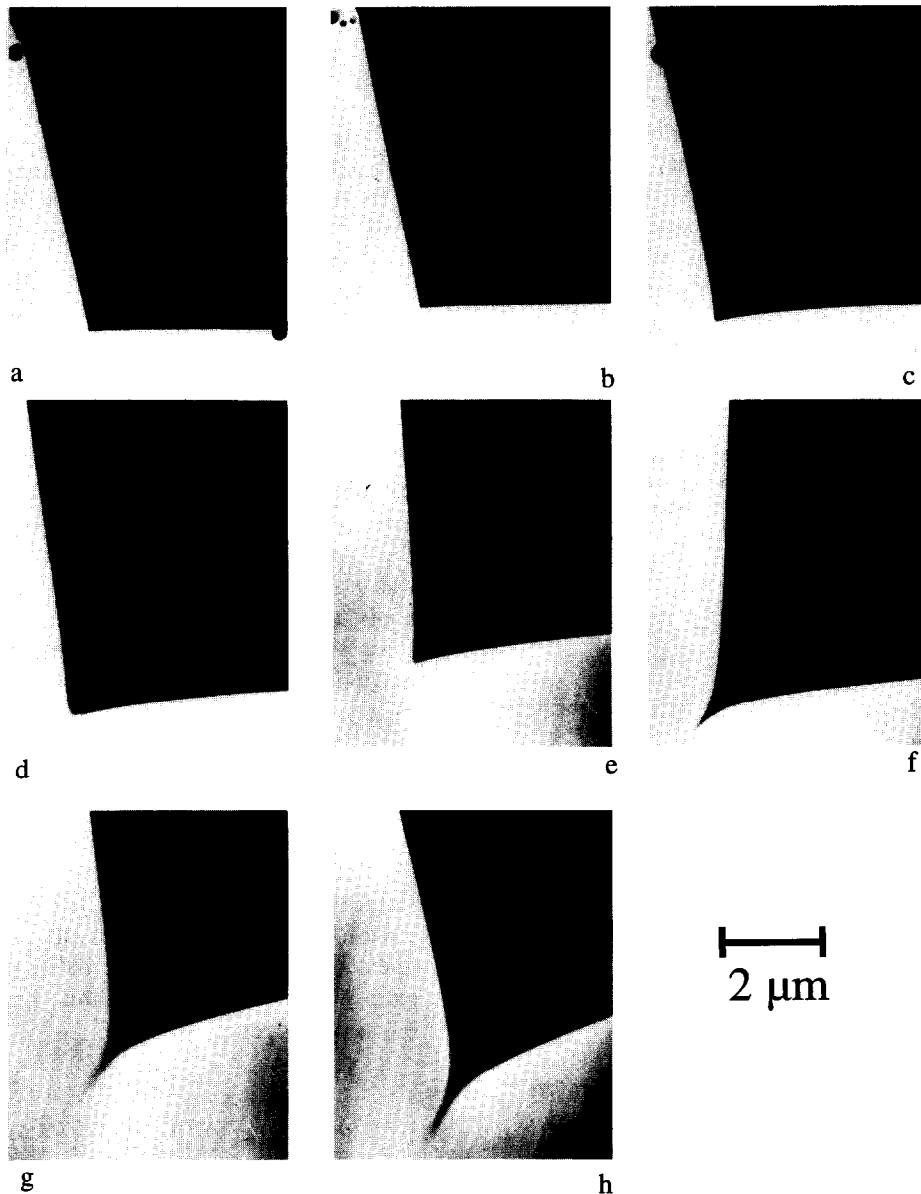


Fig. 3. Shape of the Taylor cone at different emission currents: (a)  $I_e = 2.8 \mu\text{A}$ ; (b)  $I_e = 5.1 \mu\text{A}$ ; (c)  $I_e = 10.2 \mu\text{A}$ ; (d)  $I_e = 16.5 \mu\text{A}$ ; (e)  $I_e = 21.5 \mu\text{A}$ ; (f)  $I_e = 25.5 \mu\text{A}$ ; (g)  $I_e = 31.5 \mu\text{A}$ ; (h)  $I_e = 38.5 \mu\text{A}$ .

until reaching the critical voltage  $U_T$ . It is supposed that the Taylor cone forms immediately when reaching the critical field strength (proportional to  $U_T$ ), at which the surface tension pressure cannot compensate the electric stress at the surface anymore, in order to produce a new equilibrium between both forces [7,8,13]. At the critical voltage  $U_T$  it was observed that the surface formed a bump which immediately turned into the Taylor cone. The formation steps of the cone out of the rounded surface could not be temporally resolved. That means the building time of the cone is shorter than the imaging time according to the used picture frequency. The temporal progress of the formation of the surface can be seen in Fig. 2. The temporal resolution is limited by the picture frequency of the video film.

It was possible to measure the height of the Taylor cone from the video recording. For that purpose the reluminosity of the CCD-camera,

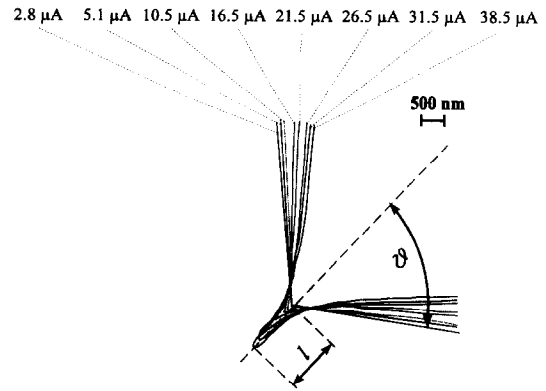


Fig. 4. Variation of the shape of the Taylor cone with increasing emission current;  $l$  and  $\vartheta$  are the length of the extension of the apex and the half opening angle of the cone, respectively.

Table 2

Variation of the cone half-angle  $\vartheta$  and the extension of the apex  $l$  in dependence from emission current  $I_e$ . (a) Experimental results for indium emission; (b) theoretical calculations by Kingham et al. [7] and by Forbes et al. [8] for gallium emission

(a)				
$I_e$ ( $\mu A$ )	$\vartheta$ (deg)	$l$ ( $\mu m$ )		
$\Delta I_e = \pm 0.3 \mu A$	$\Delta \vartheta = \pm 0.5^\circ$	$\Delta l = \pm 0.05 \mu m$		
2.8	50.4	–		
5.1	49.3	–		
10.5	48.9	0.15		
16.5	45.4	0.23		
21.5	45.8	0.45		
26.1	41.7	0.95		
31.5	41.5	1.10		
38.5	40.4	1.28		
(b)				
$I_e$ ( $\mu A$ )	Calculation by Kingham et al. [7]		Calculation by Forbes et al. [8]	
	$\vartheta$ (deg)	$l$ ( $\mu m$ )	$\vartheta$ (deg)	$l$ ( $\mu m$ )
5	49.3	0.04	45	0.0025
10	49.3	0.14	42	0.0063
15	49.3	0.22	40.3	0.015
20	49.3	0.31	38.6	0.022
30	49.3	0.5	36.8	0.042
40	49.3	0.7	34.6	0.078

which caused superimposed contours of the spherical surface and of the cone shortly after the formation of the cone (Fig. 2d), had been used. The height of the indium cone at the critical voltage  $U_T$  amounts to  $1.3 \pm 0.3 \mu m$ . The variation of the emission voltage  $U_e$  caused a shift of the image on the fluorescent screen. Therefore it was not possible to determine the height of the cone in dependence from the emission current. Figs. 3 and 4 show the shape of the Taylor cone in dependence from the emission current between 0 and  $40 \mu A$ . It is to be seen that the opening half angle  $\vartheta$  of the Taylor cone decreases with increasing emission current. Greater deviations from Taylor's value for the half angle  $\vartheta_T = 49.3^\circ$  can be observed with higher currents (Table 2). An extension of the cone apex  $l$  was stated for currents  $I_e > 10 \mu A$ . The higher the emission current the greater the extension of the apex. Fig. 5 shows that the half angle  $\vartheta$  and the extension of the apex  $l$  change linearly with the emission current:

$$\vartheta = \vartheta_0 - \frac{d\vartheta}{dI} I, \quad \text{with} \quad \vartheta_0 = 51.1 \pm 0.6 \text{ deg}$$

$$\frac{d\vartheta}{dI} = (298 \pm 29) \times 10^{-3} \text{ dcg}/\mu A, \quad (3)$$

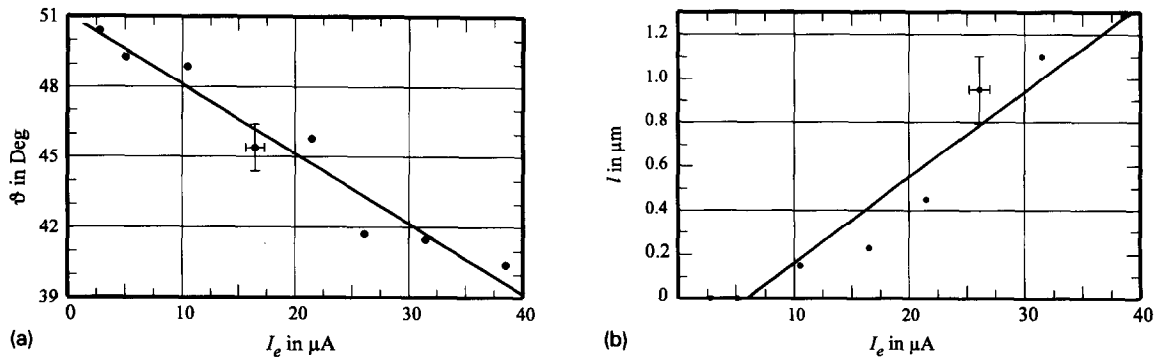


Fig. 5. (a) The cone half angle  $\vartheta$  versus emission current  $I_e$ . The fitting curve is calculated with formula (3). (b) The length of the apex extension  $l$  versus emission current  $I_e$ . The fitting curve is calculated with formula (4).

$$l = l_0 + \frac{dl}{dI} I \quad \text{with} \quad l_0 = -0.23 \pm 0.09 \mu\text{m}$$

$$\frac{dl}{dI} = (39 \pm 4) \times 10^{-3} \mu\text{m}/\mu\text{A}. \quad (4)$$

A similar behaviour could be observed by in-situ HV-TEM investigations of gallium liquid metal ion sources [21]. There, the extension of the apex of the Taylor cone  $l$  was smaller by one order of magnitude ( $5.5 \times 10^{-3} \mu\text{m}/\mu\text{A}$ ) than with indium emission. The decrease of the half angle  $\vartheta$  is smaller by a factor of 2 ( $129 \times 10^{-3} \text{deg}/\mu\text{A}$ ) [21]. These differences give conclusive evidence of the material dependence of the Taylor cone.

The apex of the Taylor cone extends continu-

ously under the influence of the outer electrostatic force and provides the equilibrium between the surface tension pressure and the electric stress also for high emission currents [14,15]. Only if this condition is satisfied can a stable cone exist for a longer time. The experiments show that changes in the field strength are not only compensated by an extension of the apex  $l$  but also by a decrease of the half angle  $\vartheta$  and a concaving of the cone surface. With emission currents over  $30 \mu\text{A}$  the concaving of the cone surface progresses so far that a linear approximation as used for the definition of the half angle is hardly possible.

This change of the cone shape may also have an indirect influence on the energy spread of

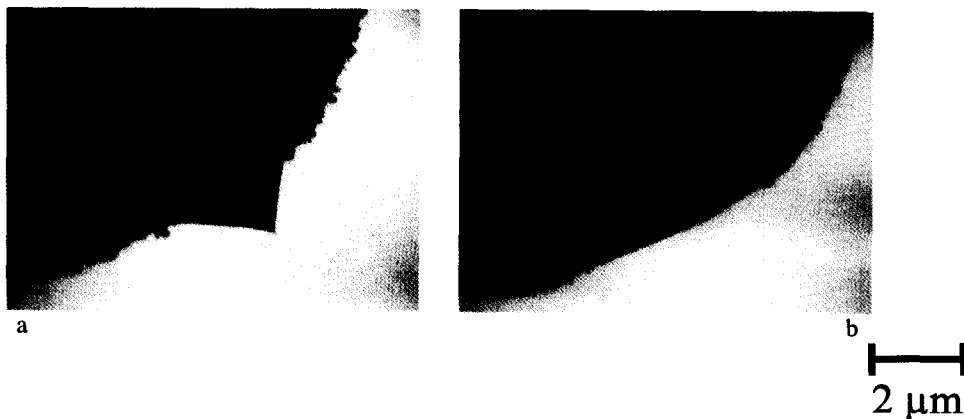


Fig. 6. Microdroplet emission from surroundings of the cone: (a) emission with  $I_e = 7 \mu\text{A}$ ; (b) no emission.

emitted ions, which is often observed experimentally [20] to be larger at higher emission currents.

#### 4. Microdroplet emission

It is known that microdroplet emission occurs with high emission currents of LMIS [2,16]. It is supposed that high frequent vibration of the liquid surface of the Taylor cone occurs with  $I_e > 20 \mu\text{A}$  (Rayleigh instability [3]) and microdroplet emission from the cone starts. The size of the microdroplets was supposed to amount up to 100 nm [18,19].

In our experiments the emission of microdroplets of this size from the Taylor cone could not be noticed, whereas microdroplet emission from the surrounding of the cone was observed (Fig. 6). The microdroplet radii vary between  $r \approx 50 \text{ nm}$  and  $r = 1.4 \mu\text{m}$  (Fig. 7) and increase with the distance from the Taylor cone (decrease of the field strength gradient). When decreasing the electrostatic field strength, and correspondingly diminishing the emission current, the forming areas of the microdroplets move closer to the Taylor cone. With a lower emission current ( $I_e \leq 5 \mu\text{A}$ ) microdroplets occasionally form on the cone's perimeter (Figs. 3a and 3b). With higher

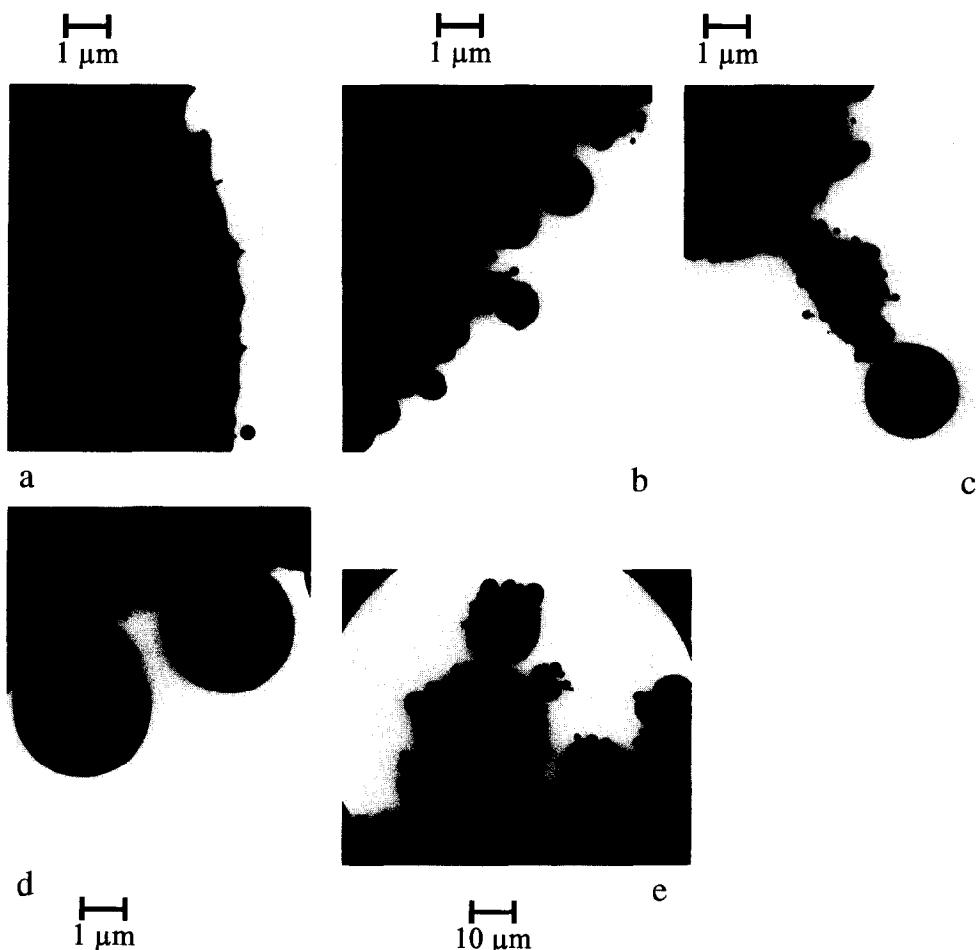


Fig. 7. Microdroplet size in dependence from the distance between their formation area and the Taylor cone. The distance to the cone increases from (a)–(e).

emission currents the liquid surface near the cone becomes smooth, and the emission areas move further away from the front side of the tip. This leads to the assumption that microdroplets form only up to a certain field strength. A shifting of the microdroplets along the liquid metal surface was not observed until their emission.

The microdroplet emission correlates with the ion emission from the Taylor cone. It starts with the cone formation and ends with the disappearance of the cone. That suggests that the microdroplet formation and emission are correlated with the liquid metal flux to the Taylor cone according to the ion emission, which comes to rest when the cone vanishes. Below the critical

voltage  $U_T$  the microdroplets are stable. Fig. 6b shows clearly that the Taylor cone is not replaced by microdroplets. The metal surface remains smooth and the emission from the surrounding is extinguished.

Fig. 8 shows a chronological series of images of the same area. The images make the microdroplet emission process evident. The frequency of the microdroplet emission decreases with the growing distance of their position from the cone. Smaller microdroplets are emitted more often than the bigger ones.

Some microdroplets are only connected to the tip by thin filaments with a diameter of approximately 70 nm (Fig. 7c). These thin filaments may

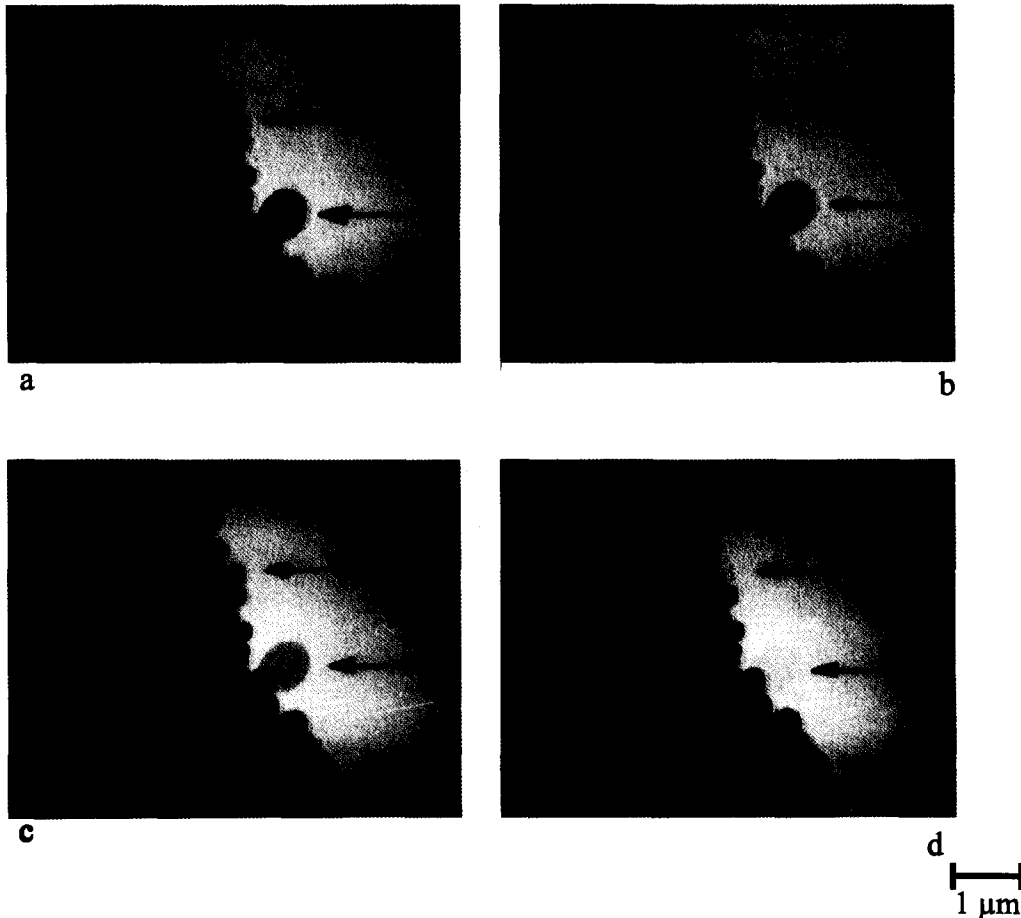


Fig. 8. Side of the emitter tip during the emission ( $I_e = 14 \mu\text{A}$ ). Images show the same area in chronological series. Arrows show the positions where microdroplets were emitted: (a) starting shoot; (b) shoot after 1 s; (c) shoot after 4 s; (d) shoot after 5 s.

exceed a length of 3  $\mu\text{m}$  and still hold stable for a long period of time.

At a greater distance from the tip (greater than 100  $\mu\text{m}$ ) other smaller microdroplets form on bigger ones, creating structures similar to little apple man (Fig. 7c). Emission from these structures was not observed.

The number of atoms per microdroplet  $n_d$  could be determined from the density of the material ( $\rho_L = 7580 \text{ kg/m}^3$  [22]) and the mass of an indium atom ( $m_{\text{In}} = 1.97 \times 10^{-27} \text{ kg}$  [23]) to be  $25 \text{ atoms/droplet} \leq n_d \leq 7.5 \times 10^5 \text{ atoms/droplet}$ . The trajectory and the stability of the microdroplets after their emission could not be

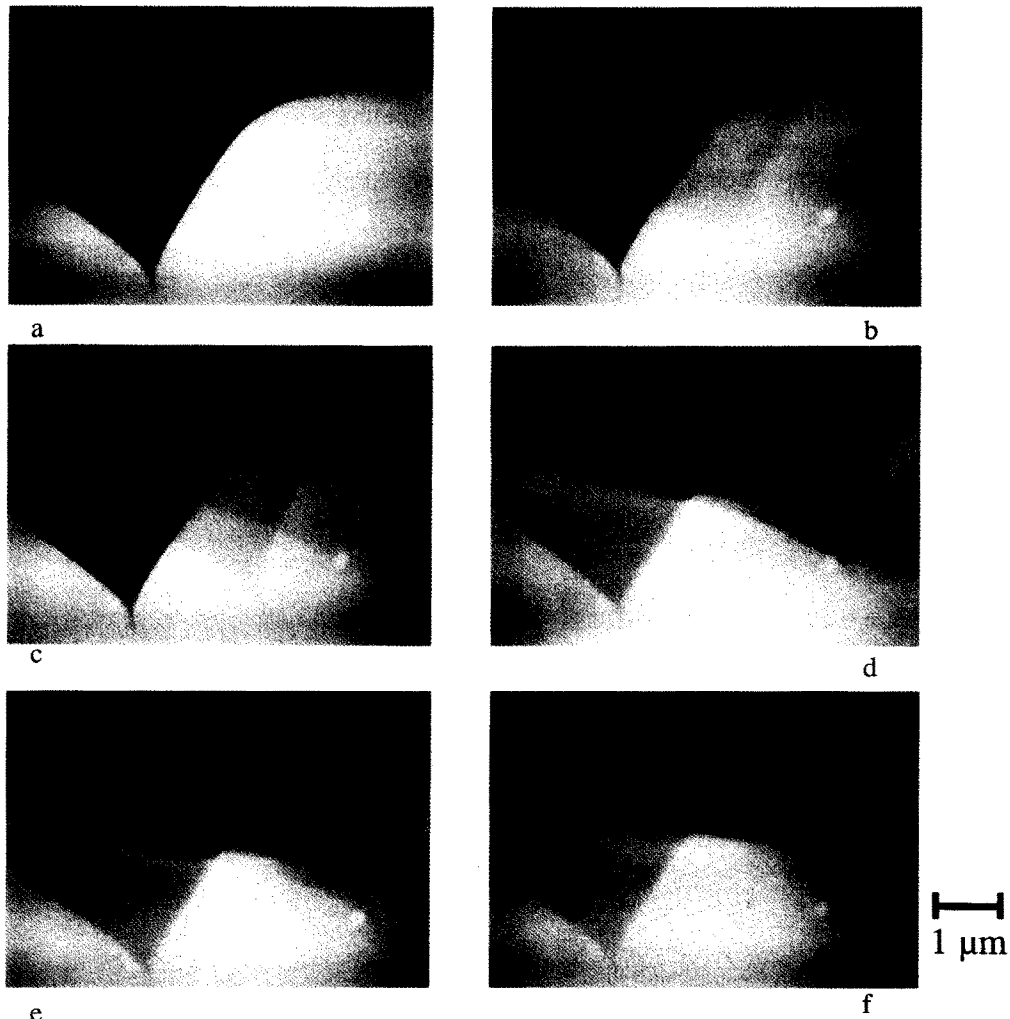


Fig. 9. Images of the double cone. (a) Starting shoot. At the beginning, a stable emission from the right cone (here outside the image) was observed. Then slowly another cone shifted sideways from the left into the image. (b) Shoot after 0.02 s. The left cone shifted fast towards the first one. Because of the reluminosity of the CCD-camera the shadow of the left cone in its starting position is visible even stronger. (c) Shoot after 0.06 s. The left cone has moved further. Several shadows of the left cone are caused by the reluminosity of the CCD-camera. (d) Shoot after 0.14 s. The left cone has almost reached the right one. Distances between shadows of the left cone become smaller. That means, the shifting velocity has decreased. (e) Shoot after 0.2 s. The cones have merged and formed a new single one. (f) Shoot after 0.24 s. The new cone emits stable. During the total process the emission current remained constant  $I_e = 21 \mu\text{A}$ .

observed because of their high velocity in relation to the picture frequency. But since the emission areas of the bigger microdroplets  $n_d > 100$  atoms/droplet were already situated at quite a distance from the front side of the tip, one can suppose that the charged microdroplets are not pulled through the electrostatic field to the Taylor cone apex, anymore. Thus these microdroplets do not contribute to the emission features of a liquid metal micro-beam probe but lead to a pollution of the extraction electrode.

The smaller microdroplets  $n_d \leq 100$  atoms/droplet can still contribute to the emission features of a micro-beam probe and influence the energy spread of an ion beam [17].

## 5. Some instabilities of the Taylor cone

In order to improve the stability of a Taylor cone it is recommended to use tips with small tip radii  $r \approx 1 \mu\text{m}$  [2,19]. Nevertheless, there is occasionally spatial shifting of the emission area which causes fluctuation of the emission current of a micro-beam probe. Fig. 9 shows the formation of a double cone and its temporal variation. At the beginning a stable emission from a cone (right in the images) was observed at the place where the maximum electric stress at the surface (on the front side of the tip) must be situated. Then another cone, whose formation had not been observed, shifted sideways from the left towards the first one until both cones suddenly merged. During this whole process the total emission current remained constant.

## 6. Summary

The formation of the indium Taylor cone and its behaviour during emission was observed in-situ in the Halle HV-TEM. The microdroplet emission from the surroundings of the Taylor cone was observed for the first time.

The half angle of the cone decreases linearly with the emission current. For emission currents  $I_e > 10 \mu\text{A}$  an extension of the cone apex was

observed. This extension grows according to the emission current and can exceed  $1 \mu\text{m}$ .

The microdroplet emission in the surrounding of the Taylor cone shows an unexpected intensity. The size of the microdroplet increases with diminishing field strength gradient. Their radii vary from  $0.045$  to  $1.4 \mu\text{m}$ . The emission frequency of the microdroplet is inversely proportional to their size. The physical principle of the microdroplet emission in the surrounding of the Taylor cone has not been clarified yet.

During constant ion emission, dynamic processes at a double cone were observed.

## Acknowledgements

The authors would like to thank Professor J. Heydenreich (Max-Planck-Institut für Mikrostrukturphysik Halle) and the Deutsche Forschungsgemeinschaft for their support concerning these investigations. Moreover, we thank Mrs. F. Pabisch (Max-Planck-Institut für Mikrostrukturphysik Halle) for contributing valuable experience in preparation and testing of the liquid metal ion emitters. We also thank Professor R.G. Forbes (University of Surrey) and Professor T. Mulvey (Aston University Birmingham) for stimulating discussions and the referees for most helpful remarks.

## References

- [1] J. Melangelis, *J. Vac. Sci. Technol. B* 5 (1987) 469.
- [2] P.D. Prewett and G.L. Mair, *Focused Ion Beams from Liquid Metal Ion Sources* (Research Studies Press Ltd., Wiley, New York, 1991).
- [3] Lord Rayleigh, *Philos. Mag. Ser. 5*, 14 (1882) 184.
- [4] J. Zeleny, *Phys. Rev.* 10 (1917) 1.
- [5] G.I. Taylor, *Proc. Roy. Soc. (London) A* 280 (1964) 383.
- [6] R. Gomer, *Appl. Phys.* 19 (1979) 365.
- [7] D.R. Kingham and L.W. Swanson, *Appl. Phys. A* 34 (1984) 123.
- [8] R.G. Forbes and N.N. Ljepojevic, *Surf. Sci.* 266 (1992) 170.
- [9] G. Benassayag, P. Sudraud and B. Jouffrey, *Ultramicroscopy* 16 (1985) 1.
- [10] E. Müller and T.T. Tsong, *Field Ion Microscopy – Principles and Applications* (Elsevier, New York, 1969).

- [11] G. Möllenstedt and H. Düker, *Z. Phys.* 145 (1956) 377.
- [12] L.D. Landau and E.M. Lifschitz, *Lehrbuch der Theoretischen Physik*, Vol. 2 (Akademie-Verlag, Berlin, 1987).
- [13] G.L.R. Mair and T. Mulvey, *Scanning Electron Microsc.* 4 (1984) 1531.
- [14] G.L.R. Mair and R.G. Forbes, *Surf. Sci.* 266 (1992) 180.
- [15] R.G. Forbes and N.N. Ljepojevic, *Surf. Sci.* 246 (1991) 113.
- [16] P. Joyes, J. van de Walle and C. Colliex, *Ultramicroscopy* 20 (1986) 65.
- [17] R. Hornsey and T. Ishitani, *Jpn. J. Appl. Phys.* 6 (1990) L1007.
- [18] V.V. Vladimirov, V.E. Badan and V.N. Gorshkov, *Surf. Sci.* 266 (1992) 185.
- [19] P.D. Prewett and E.M. Kellogg, *Nucl. Instrum. Methods B* 6 (1985) 135.
- [20] R. Hornsey, *Jpn. J. Appl. Phys.* 30 (1991) 366.
- [21] W. Driesel, Ch. Dietzsch, H. Niedrig and B. Praprotnik, to be published.
- [22] C.A. Hampel, *The Encyclopaedia of the Chemical Elements* (Reinhold, New York, 1968).
- [23] *Gmelins Handbuch der Anorganischen Chemie*, 8 Auflage, System-Nummer 36 (Verlag Chemie, Berlin, 1936).
- [24] R.G. Forbes, private communications.